NASA
TP
1910
c.1

NASA Technical Paper 1910

LOAN COPY: R
AFWL TECHNI
KIRTLAND AFE
0067685
TECH LIBRARY KAFB, NM

Viscous-Inviscid Interaction Method Including Wake Effects for Three-Dimensional Wing-Body Configurations

Craig L. Streett

SEPTEMBER 1981

FOR EARLY DOMESTIC DISSEMINATION
Because of its significant early commercial potential, this information, which has been developed under a U.S. Government program, is being disseminated within the United States in advance of general publication. This information may be duplicated and used by the recipient with the express limitation that it not be published. Release of this information to other domestic parties by the recipient shall be made subject to these limitations.
Foreign release may be made only with prior NASA approval and appropriate export licenses. This legend shall be marked on any reproduction of this information in whole or in part.
Review for general release September 30, 1983

NASA

TECH LIBRARY KAFB, NM
0067685

NASA Technical Paper 1910

Viscous-Inviscid Interaction Method Including Wake Effects for Three-Dimensional Wing-Body Configurations

Craig L. Streett
Langley Research Center
Hampton, Virginia

National Aeronautics
and Space Administration

**Scientific and Technical
Information Branch**

1981

SUMMARY

An existing three-dimensional compressible integral boundary-layer method was modified to account for mean dilatation effects, to model transition properly, and to provide better numerical stability near computational boundaries. Results of this method were compared with those from a three-dimensional finite-difference boundary-layer method on a difficult test case. An interaction procedure was developed to couple this integral method with a number of wing-alone and wing-body transonic potential codes to account for viscous effects. A locally two-dimensional wake model, including thickness and curvature effects, was developed and incorporated into this interaction procedure. Results from this procedure were compared with experimental data and results from previous procedures for test cases where viscous effects were large.

INTRODUCTION

It is now generally recognized that any analysis procedure for computing transonic flow over wing and wing-body configurations must include some form of viscous correction on the wing to give reasonable agreement with experiment. A number of researchers have shown good agreement without viscous correction through the use of lift-matching; however, such techniques require a priori knowledge of the overall lift, rather than it being a computational result. Ideally, one would like to compute flows using only known geometric quantities and flow conditions. Some form of viscous correction thus appears to be required.

Techniques for solving the Navier-Stokes equations, either in full form or in some reduced form (parabolized, velocity split, etc.), are still in their infancy. In addition, Navier-Stokes computations for a transonic wing at Reynolds numbers of interest are still beyond the capability of present computers. Alternatively, potential-flow and boundary-layer computational techniques are mature, and the viscous-inviscid interaction philosophy of computing flow fields with viscous effects has been applied successfully in the past to problems of interest.

Viscous-inviscid interaction consists of iteratively solving the boundary-layer and potential (or other inviscid flow) equations, coupled through the concept of boundary-layer displacement thickness. If the Navier-Stokes equations are written in terms of matched asymptotic expansions near and far from a wall, it can be shown that to $O(N_{Re}^{-1/2})$ the pressure on the wall is determined from the solution of the outer (inviscid) equations, with the flow tangency boundary condition displaced from the wall by a distance determined from the inner (boundary-layer) equations. This viscous-inviscid interaction technique produces a uniformly valid solution, with the exception of strong interaction regions, for example, near the trailing edge, a normal shock, or the wing tip.

Melnik, Chow, and Mead (ref. 1) have shown in two dimensions that this interaction of the first-order equations involves a singularity in the pressure gradient and streamline curvature at the trailing edge of an airfoil. It has been demonstrated computationally, however, that iterating the boundary layer and potential equations until convergence produces a self-consistent solution in which this singularity does not appear. It is shown in reference 2 that although this self-consistent solution is not singular, it is inconsistent with the normal momentum equation in a small region near the trailing edge. Correction to the inviscid boundary conditions near the trailing edge in two dimensions is developed in reference 1 to account for this inconsistency; a similar development for three-dimensional wings with spanwise flow at the trailing edge is not available. Although self-consistent interaction solutions are not rigorously accurate to first order near the trailing edge, such solutions do show good agreement with experiment. Such a self-consistent development is described in this paper.

There are several boundary-layer schemes which may be applied to an interaction procedure. Several researchers (refs. 3 to 5) have demonstrated fair agreement with experiment by using two-dimensional boundary-layer calculations applied in chordwise strips over the wing span. However, experiments with modern transport wings with moderate sweep, utilizing supercritical airfoil sections, show large amounts of spanwise flow in the lower surface cove region. This flow tends to relieve the mass buildup in the lower surface boundary layer near the root and increase it near the tip. Strip theory would then predict more viscous decambering near the root and less near the tip than a method which accounts for this cross flow. When this effect is significant, a fully three-dimensional viscous correction should provide improved accuracy compared with two-dimensional strip theory.

A number of finite-difference procedures have been developed to compute wing boundary layers in three dimensions, such as the one described in reference 6. These methods still require considerable empiricism in the form of a turbulence model, and they are expensive to run. These codes also tend to be quite difficult to use in an interactive scheme, as primary flow separation and inflow at a boundary are often too destabilizing computationally for the procedure to withstand. Thus the boundary-layer procedure may fail to give a solution in some region of the wing so that further global iterations are impossible. This situation can occur even when the predicted boundary layer at convergence is well-behaved.

Three-dimensional integral methods are less complex and more reliable than the finite-difference methods but present a more physically reasonable description of the three-dimensional boundary layer than the two-dimensional strip methods. In general, integral methods are characterized by replacing detail velocity profile calculations with assumptions of general profile shapes or families. These profile families are characterized by one or more integral parameters, such as momentum thickness and shape factor. In the three-dimensional case, the boundary layer is split into streamwise (i.e., parallel to the external streamline) and cross-flow (perpendicular to the external streamline) components, as was suggested by Coles (ref. 7). These profile assumptions are substituted into the governing equations, which are in turn integrated across the boundary layer in the wing surface normal direction. Thus, the three-dimensional boundary-layer equations are converted into a

set of two-dimensional equations in the planform plane for the unknown integral parameters.

The three-dimensional integral boundary-layer method used in this work was based on a code developed by the German aerospace firm, Dornier G.m.b.H. (ref. 8). A description of the method, along with the modifications incorporated into it during this study, appears in a later section. Results from this code are compared with those of a three-dimensional finite-difference boundary-layer code. The interaction of this code with two transonic full-potential wing-alone codes and one wing-body code is described, and results for two transport wing-body test cases with supercritical airfoil sections are shown. For one test case, overall viscous effects, body effects, and influence of different wake treatments are described.

It is shown in this paper that, by including the effects of wing surface boundary layer and both wake displacement and curvature, wing lift distribution and shock position are predicted well. However, since the strong viscous-inviscid interaction of the trailing-edge region is not modeled properly, trailing-edge pressures are generally predicted too high. The drag predicted by this method, which accounts only for weak interaction, thus is in error. It is shown in reference 1 for two-dimensional airfoil flow that the trailing-edge strong interaction region must be accounted for to obtain accurate drag prediction.

SYMBOLS

a_e speed of sound at edge of boundary layer

a_o stagnation speed of sound

A aspect ratio

b semispan

c local chord

c_l local section lift coefficient

C_p pressure coefficient

DFVLR Deutsche Forschungs- und Versuchsanstalt für Luft- und Raumfahrt E.V.

G reduced potential used in inviscid codes

$\bar{H}$ streamwise shape factor, $\equiv \delta_1^*/\theta_1$

M Mach number

N_{Re} Reynolds number per unit length

$N_{Re,c}$ Reynolds number based on chord

R normalized lift reduction due to viscous effects

s_w arc length along wake

t maximum section thickness

u local boundary-layer velocity in external streamwise direction

U external velocity magnitude

v local boundary-layer velocity normal to external streamwise direction

x chordwise coordinate

y spanwise coordinate

z physical normal coordinate

Z transformed normal coordinate

β angle between external streamline and wall shear direction

Γ_w wake vorticity

δ^* total boundary-layer displacement thickness

δ_1^* streamwise displacement thickness, $\equiv \int_0^\infty \left(1 - \frac{\rho}{\rho_e}\frac{u}{U}\right) dz$

δ_2^* cross-flow displacement thickness, $\equiv \int_0^\infty \frac{\rho}{\rho_e}\frac{v}{U}\, dz$

δ_w^* wake displacement thickness, $\equiv \int_{-\infty}^\infty \left(1 - \frac{\rho}{\rho_e}\frac{u}{U}\right) dz$

Δ transformed boundary-layer thickness

ε local flow angle in constant-span plane

η normalized spanwise coordinate, $\equiv y/b$

θ_1 streamwise momentum thickness, $\equiv \int_0^\infty \frac{\rho}{\rho_e} \frac{u}{U}\left(1 - \frac{u}{U}\right) dz$

θ_w wake momentum thickness, $\equiv \int_{-\infty}^\infty \frac{\rho}{\rho_e} \frac{u}{U}\left(1 - \frac{u}{U}\right) dz$

κ_w wake curvature

$\Lambda_{c/4}$ quarter-chord sweep angle

ρ local density

ρ_e density at edge of boundary layer or wake

ρ_o stagnation density

BOUNDARY-LAYER METHOD AND VERIFICATION

The boundary-layer method used in this study was obtained from Dornier G.m.b.H.; it is based on the laminar scheme developed in reference 8 and the turbulent method described in reference 9, with a number of modifications. Details of the development of these schemes is not given herein; rather, a general description and discussion of assumptions and their effects follow.

Boundary-Layer Analysis

For purposes of analysis, the boundary layer is decomposed into components parallel and perpendicular to the external streamline. A basic schematic of this decomposition of the boundary layer is shown in figure 1. The situation shown is that most commonly encountered, in which the cross-flow velocity does not change sign across the boundary layer.

The laminar analysis used in this study is basically unchanged from that developed in reference 8. The streamwise velocity profile is assumed to be of the Faulkner-Skan family of similarity profiles. The cross-flow profile is generated from a linear combination of these similarity profiles; this combination is capable of generating profiles with cross-flow velocity crossover. These profiles are defined for incompressible flow; the Stewartson transformation is used to scale the normal coordinate:

$$dZ = \frac{\rho a_e}{\rho_o a_o} dz$$

By this transformation, the compressible velocity profile may be represented by the incompressible form, as a function of the transformed variable Z.

These profile assumptions are substituted into the two boundary-layer momentum equations and their corresponding moment of momentum relations. The moment relations are often used in integral boundary-layer methods (ref. 10); they are independent relations formed by multiplying the momentum equations by the distance from the wall. These four equations are then integrated from the wall to the boundary-layer edge. The resultant equations form a system of four coupled partial differential equations in two dimensions on the surface of the wing for four unknowns; the four unknowns are parameters related to the streamwise momentum thickness, the wall shear, the cross-flow displacement thickness, and the boundary-layer thickness. The streamwise momentum thickness is defined as

$$\theta_1 = \int_0^\infty \frac{\rho}{\rho_e} \frac{u}{U}\left(1 - \frac{u}{U}\right) dz$$

and the cross-flow displacement thickness as

$$\delta_2^* = \int_0^\infty \frac{\rho}{\rho_e} \frac{v}{U} dz$$

In the turbulent case, a simple power-law profile is assumed for the streamwise direction in the form

$$\frac{u}{U} = \left(\frac{Z}{\Delta}\right)^{n(\bar{H})}$$

where Z is the transformed normal coordinate, and the exponent n is a function of the streamwise shape factor $\bar{H}$. The cross-flow profile used was suggested by Mager (ref. 11) as follows:

$$\frac{v}{U} = \frac{u}{U}\left(1 - \frac{Z}{\Delta}\right)^2 \tan \beta$$

where β is the angle between the external streamline and the wall shear direction. Note that this relation cannot predict a cross-flow profile with velocity crossover.

These profiles are substituted into the boundary-layer momentum equations and integrated, as before; a modified Ludwieg-Tillmann relation is used to evaluate the wall shear (ref. 12). To close the system of equations, an integral continuity equation is formed, in which the change in mass flow in the boundary layer is explicitly identified. This change in mass flow, the so-called entrainment coefficient, is related to the other integral quantities through the lag-entrainment concept of Green et al. (ref. 13). Thus, in the turbulent case, a set of three coupled first-order PDE's is generated for the streamwise momentum thickness, the shape factor, and the wall shear angle. The use of the lag-entrainment relations, rather than a local entrainment equation is the difference between the method used in this study and that described in reference 9.

For a three-dimensional boundary layer, the displacement thickness must be computed as a solution to a PDE on the surface, rather than being computed from a local integral as in the two-dimensional case. In both the laminar and turbulent methods, therefore, an a posteriori solution of the integrated continuity equation yields the displacement thickness.

Rather than using a streamline coordinate system, as is usually done in three-dimensional boundary-layer calculations, a simple wing constant-chord constant-span system is used. Although nonorthogonal, this system alleviates the difficulty of having to generate a complex new coordinate system for each viscous-inviscid iteration. The additional terms from the nonorthogonal transformation are not computationally time-consuming because the systems of equations are first order; therefore, this coordinate system is considered more efficient than streamline coordinates for the integral methods. A schematic representation of the coordinate system used is given in figure 2.

The three-dimensional boundary-layer equations display hyperbolic properties in the planform plane; that is, at any point on the plane, the equations have a domain of dependence which must be honored in any numerical solution scheme. The integral equations have the same property. It is shown in reference 14 that the characteristics of the turbulent integral equations always lie between the external streamline and the wall shear line, giving a convenient, conservative approximation to the exact domain of dependence.

An explicit finite-difference scheme is used to march the solution of the coupled system of equations in the chordwise direction. Differencing of quantities in the y-direction (spanwise) must be upwind to properly account for the domain of dependence. That is, if both the external streamline and wall shear line extend to the same side of the chord line from a computational point, the spanwise difference must be taken as one-sided from the opposite side. If the external streamline and wall shear line lie on opposite sides of the chord line, a central difference is used for the spanwise derivative. In addition, the step size in the x-direction (chordwise) is limited by the Courant-Friedricks-Lewy (CFL) condition, a necessary condition for the stability of an approximate solution scheme for a hyperbolic equation (ref. 15).

The spanwise differencing scheme of reference 14 must be modified at the wing root and tip, when flow into the computational region occurs at these boundaries, in order to make the procedure more reliable. Strictly, initial conditions must be provided at these locations. None being available, conditions along the boundaries must be assumed in these cases if the numerical scheme is to be stable. At the wing root, a plane of symmetry is assumed. Thus, on this chord line, the cross-flow velocity is set to zero, as are all spanwise derivatives. Such an assumption is at least a reasonable model of the physical situation. During the course of the present study, this wing-root boundary condition was also approximated using infinite swept-wing assumptions, that is, spanwise derivatives only set to zero. This boundary condition, however, was not found to be strong enough to be reliable for general use.

The wing-tip boundary is considerably more difficult. For this study, the assumption of zero spanwise derivatives on the tip chord line is used when flow into the region along this boundary is signaled. This is equivalent to assuming locally that the tip is part of an infinite swept wing. This assumption was found to be the weakest condition of those examined that was always stable and gave the least disturbance across the span. The inviscid method does not accurately model the outer flow in the tip region because of assumptions made concerning the shape of the trailing vortex sheet; therefore, the boundary-layer assumption made in the tip region is not considered restrictive.

The initial condition along the leading edge is provided by an approximate attachment line analysis, such as that contained in reference 16. The attachment line is assumed to be along the wing leading edge. Transition location is input, fixed along a span line at that fraction chord. The transition model was modified from the original boundary-layer code obtained from Dornier to enforce continuity of the displacement thickness at transition. There is no inconsistency in this assumption as there would be in many two-dimensional integral methods because δ^* is not an integral parameter of either the laminar or the turbulent method but is developed from a separate integration of the continuity equation.

Separation is signaled in the streamwise direction when integral parameters reach critical values; in the laminar case, when the transformed wall shear reaches zero; and in the turbulent case, when the streamwise shape factor reaches 2.4. No cross-flow separation model is used. When laminar separation is detected along a chord line, transition is assumed over the entire span. If separation is signaled at a point in a turbulent region, the streamwise shape factor, skin friction, and wall shear angle are frozen thereafter along that chord line, and spanwise derivatives are set to zero. A one-dimensional integration of the integral equations is thereafter performed on this chord line. This is considered an extrapolation technique; it should be understood that the integral equations with the given profile assumptions are invalid in large regions of separation. However, this method is assumed to give at least a reasonable solution in this situation and is required since such separated regions often appear only during the early iterations of the viscous-inviscid interaction. If the boundary-layer method were to stop at separation, the iteration procedure could not continue. If the interaction scheme converges to a solution with large separation regions remaining, the underlying assumption of the existence of a thin viscous region is invalid.

Modifications were also made to the lag-entrainment calculations in order to improve the δ^* predictions. First, the streamwise pressure gradient was correctly incorporated into the equations which were originally developed for the two-dimensional case. Second, a modification to the dissipation length scale, due to dilatation of the compressible flow, was applied (ref. 13). The effects of these modifications are seen only in regions of severe pressure gradient or large cross flow.

Verification of Boundary-Layer Method

In order to gain confidence in the integral boundary-layer method, a rather severe test case was run for comparison with results from the three-dimensional finite-difference boundary-layer method described in reference 6. The velocity data input to both boundary-layer codes was a final converged interacted solution for the flow about a swept, tapered transport wing with significant aft camber. The interaction procedure used to produce this solution is the topic of later sections of this report; details of this procedure are not important here. A converged solution was used as input since the finite-difference code of reference 6 was unable to produce a boundary-layer solution over so much of the wing surface that comparisons were meaningless when the inviscid, uninteracted velocity distribution was input.

Figure 3 shows the difference in the displacement thickness predictions of the original Dornier three-dimensional integral boundary-layer code and the code modified for use in this study. Differences are seen near transition (which for this case occurred at 0.17 c), after the shock near midchord on the upper surface, at the upper surface trailing edge, and in the cove region on the lower surface.

A comparison of the displacement thickness predictions of the modified integral method and of the finite-difference scheme of reference 6 is given in figure 4. The span station at which this comparison is made is near midspan since assumptions made at the wing root and tip are different for the two methods. The agreement shown at this midspan station is typical for most of the wing. The largest percent difference is just aft of the midchord shock. The two methods also agree well on the location of the small upper surface trailing-edge separation region and on the wall shear angle in the lower surface cove region. Even the skin-friction coefficient predicted by the integral method is within 10 percent of that predicted by the finite-difference code, despite the very crude skin-friction model used in the integral method. The finite-difference code required almost 3200 CP seconds on the Control Data CYBER 173 Computer System to produce a boundary-layer solution for this test case, whereas the integral code required less than one-thirtieth of this time and used about one-half the core storage.

Results of the three-dimensional integral boundary-layer method were also compared with experimental data. Although three-dimensional test cases were desired, cases with adequate coverage of velocity data could not be found. In principle, the two momentum equations and the continuity equation could be solved in the planform plane at the edge of the boundary layer to derive the external velocity distribution given the surface pressure. However, such a

scheme requires fixing a set of rather arbitrary boundary conditions, especially at the critical tip region which can be an inflow boundary for the upper surface. In addition, the equations are first order and were found to be quite sensitive to the applied boundary conditions; this scheme was thus dropped after some effort, and some two-dimensional test cases were run.

Perhaps the most representative and difficult two-dimensional test case was that of the upper surface boundary layer on the CAST 7 airfoil as tested in the DFVLR 1 × 1 meter tunnel (ref. 17). The case included a moderately strong shock and some separation at the trailing edge. The test and calculation were run at a Mach number of 0.76 and a Reynolds number of 2.4×10^6. Calculation was begun from measured momentum thickness and shape factor at 30 percent chord. Figure 5 shows the measured pressure distribution and the measured and computed momentum thickness distributions. The rapid thickening of the boundary layer in the high adverse pressure gradient region of the shock is predicted well, as is the thickness at the trailing edge. Proper prediction at the trailing edge is quite important, as lift is greatly influenced by the trailing-edge angle of the displacement body. Note the slight postshock disagreement due, perhaps, to the lack of a proper shock—boundary-layer interaction model. However, since the experiment shows the thickness reducing in a region of zero pressure gradient, one must also suspect some three-dimensional relief in the experiment, perhaps the shock curving back near the sidewalls.

Although the physical modeling of the boundary-layer flow is far more accurate in finite-difference methods, it is believed that this integral method, capable of producing solutions in reasonable agreement with a good finite-difference code in far less computer time, is a powerful tool for engineering calculations. Predictions of the integral method also agree well with experiment. The advantage of greatly reduced computation time, along with considerable robustness, makes the integral boundary-layer method well suited for use in interaction schemes.

INVISCID ANALYSES

During the course of this study, the boundary-layer method described in the previous section was interacted with a number of inviscid analysis codes. The three codes primarily used were of the FLO series, authored mainly by Jameson and Caughey (refs. 18 to 21). All three solve the full-potential equation, but in different forms or in different coordinate systems. This study was initiated using FLO-22, written for "wing only" configurations; no results for interactions using FLO-22 are presented in this paper. FLO-27, a wing-cylinder code, and FLO-30, a more general wing-body analysis code, were also used. Most of the interacted results presented here have been obtained using FLO-30.

FLO-22 is the oldest code and, thus, is somewhat more well-tried than the others. The boundary-conforming grid used in FLO-22 is produced by shearing out the wing sweep, then applying a parabolic mapping, and finally shearing out the wing thickness. A planar vortex sheet is assumed. The full-potential equation is written in a nonconservative finite-difference form, using Jameson's "locally rotated" (ref. 18) operators. Solution is by line successive over-relaxation

(LSOR) with user-preset grid halving. As with all potential equation methods, good approximation is expected only in flows with weak shocks. Also, the nonconservative formulation produces solutions which do not maintain mass conservation through a shock. The effect of the nonconservative form is usually seen in the incorrectly predicted shock position.

FLO-27 uses a finite-volume scheme to produce conservative differencing of the full-potential equation. After a preliminary Joukowsky transformation in the cross-flow plane, which maps the cylindrical fuselage onto a vertical slit, the grid is generated in a manner similar to that in FLO-22, although another shearing transformation is applied to remove wing taper to maintain a constant number of grid points at each span station. Solution is again by LSOR, with additional iterative damping in the form of the mixed space-time derivative added to stabilize the scheme. Although the difference form used in FLO-27 is a better approximation than that in FLO-22, convergence is somewhat slower. Also, the finest grid used in FLO-27 is coarser than that in FLO-22 although FLO-27 requires more core storage. In all, FLO-27 was found to be about 10 percent more expensive to run than FLO-22 in these interaction studies.

Most of the interaction logic was developed and initial operating experience was gained by using FLO-27 for inviscid analysis. As shown later, however, the effect of the body on the inviscid flow is large for practical configurations. This necessitated the application of the developed interaction logic to a wing-body analysis code; FLO-30 was obtained for this purpose. The differencing and solution of the full-potential equation as used in FLO-30 is quite similar to that in FLO-27, in which a finite-volume scheme in conservative form is used. The coordinate system used, described in reference 19, is termed the "wind-tunnel" grid. Coordinates in the cross-flow plane are cylindrical, normalized with the fuselage section variation sheared out. A conformal mapping is used to "unwrap" constant-radius surfaces about the wing/wake surface similar to parabolic coordinates. As a last step in the grid-generation procedure, the wing thickness is sheared out. As with all finite-volume coordinate systems, grid extent is finite.

In order to model the effect of the boundary layer on the outer inviscid flow, the displacement thickness computed by the boundary-layer method was added to the basic wing shape in the surface normal direction. This technique was used, as opposed to using surface transpiration boundary conditions, for simplicity of incorporation into the FLO codes. The techniques are mathematically equivalent to $O(N_{Re}^{-1/2})$ (refs. 22 and 23), although some researchers have reported differences in results in practice (ref. 5). The displacement thickness distribution is under-relaxed between iterations to prevent oscillations in total lift and lift distributions in the inviscid calculations. In addition, chordwise constant-value extrapolation is sometimes used on the first iteration when separation is predicted in the cove region of the lower surface; this was found to speed convergence greatly in difficult cases.

The wake in the FLO codes is modeled as a contact discontinuity, across which the pressure is continuous but tangential velocity discontinuous. The small-disturbance form of this condition leads to a constant potential jump being carried downstream from the trailing edge on constant-span lines, with the value of the potential jump determined by using potential values at the

trailing edge. An approximate wake center-line shape is used, dependent on the wing trailing-edge angle, and is sheared out along with the wing surface shape during the coordinate generation process. This procedure fixes the wake along a coordinate surface to simplify the application of the wake boundary conditions.

WAKE TREATMENT

One major purpose of this work was to study the effect of the wake approximation used. A full, asymptotically correct wake treatment for three-dimensional wing configurations of the kind described in reference 1 for two dimensions is at the present time lacking. However, displacement and curvature were the first wake effects accounted for in two-dimensional studies (ref. 22); therefore, a similar treatment is given here.

For this study, the wake model used in the original FLO-30 code was replaced with one satisfying flow tangency on the wake displacement body and the pressure jump condition from wake curvature. As on the wing surface, the solid displacement surface model was used for the wake, constructed in two-dimensional strips. The pressure jump across the wake displacement body, related to the streamline curvature and momentum thickness of the wake, was reformed into a condition on the change in potential jump along the wake, as in reference 1.

A fixed approximation to the wake center-line location was used for simplicity. This surface leaves the trailing edge smoothly at the averaged local trailing-edge angle, and the angle between the wake center-line surface and free-stream decays logarithmically as the general streamline shape of a point vortex in uniform flow. Wake displacement thickness was then applied along this surface.

The flow curvature at the actual wake was computed from the rate of change of the flow angle along the fixed wake; that is,

$$\kappa_w = \frac{d\varepsilon}{ds_w}$$

Here, as in reference 1, the approximation is made that the actual wake lies close to the preset inviscid wake near the trailing edge where the curvature effect is significant. An alternate approximation from inviscid theory was tried:

$$\kappa_w = -\left(\frac{1}{u}\frac{du}{dz}\right)_w$$

where z is the direction normal to the wake. However, the cell spacing in the normal direction was found to be too large, and the curvature computed from the

expression was too low near the trailing edge. This being the region where wake curvature effects are largest, the normal derivative expression for the curvature was dropped. Following reference 1, the wake potential jump condition is

$$\frac{d\Gamma_w}{ds_w} = -\theta_w \kappa_w$$

with $\Gamma_w = [\![G]\!]_w \equiv G_u - G_\ell$ at the wake (where the subscripts u and ℓ indicate upper and lower, respectively).

The integral properties of the wake were computed during the same stage of the interaction iterations as the boundary-layer calculations. A compressible lag-entrainment method, outlined in reference 13, was used to compute δ^*_w and θ_w on streamwise strips, with boundary-layer conditions along the trailing edge used as initial conditions. Two separate wake computations were made at each span station, for either side of the wake center line; the total integral properties of the wake are then the sum of the corresponding properties from both sides.

INTERACTION PROCEDURE

Viscous-inviscid interaction results were produced in this study by iterating potential, boundary-layer, and wake solutions until overall convergence was obtained. A cycle, or "global iteration" of this process, consists of computing the external inviscid flow over the displacement surface of the wing and wake, with the inviscid wake potential jump condition modified by the curvature condition described previously, and, subsequently, of updating the viscous parameters by boundary-layer and wake calculations, using the external velocity distributions previously computed. The updated viscous parameters then provide a new displacement surface for the inviscid calculation of the next global iteration. In practice, the displacement surface updates must be underrelaxed with the viscous parameters of prior cycles to minimize oscillations. The computed displacement thickness on the wing is smoothed to give the displacement surface continuous curvature. Also, the inviscid calculations within each global iteration are stopped short of convergence within the potential equation iterative solution scheme. This practice was found to reduce the overall work involved in achieving global convergence.

The potential codes described previously require very large amounts of computer storage. The finest grids used in FLO-22, FLO-27, and FLO-30 were (192 × 24 × 32), (161 × 18 × 35), and (161 × 24 × 32), respectively. Because of this, the integral boundary-layer code and interpolating codes required to process velocity and displacement thickness data were kept as separate routines. The interaction iterations and flow of information between these programs were controlled by a job stream using the powerful CDC CYBER Control Language (CCL).

RESULTS

Experimental Configurations

In order to show the advantages of the present more complete wake treatment, as opposed to the treatments previously used for three-dimensional wing calculations, configurations for which viscous effects are large must be used. The first test case chosen was selected from a family of supercritical wings tested at the Langley Research Center for advanced transport configurations (ref. 24). The specific wing-body configuration used here is also one of the cases given in reference 4. A photograph of the wind-tunnel model, mounted for testing in the Langley 8-Foot Transonic Pressure Tunnel, is shown in figure 6, and a line drawing of the configuration is given in figure 7(a). The wing is of relatively high-aspect ratio and is swept and tapered. Supercritical airfoil sections with large aft camber are used over the span; a small amount of twist is employed, and the thickness ratio varies from 0.144 at the root to 0.106 at the tip. The wing is mounted in a low position on a relatively wide body.

In the second test case, a somewhat lower aspect-ratio wing is mid-mounted on a cylindrical fuselage. A schematic of this configuration is shown in figure 7(b). Viscous effects for this case are less than on the first test case configuration, but a shock of greater strength appears on the upper surface for similar free-stream Mach number and overall lift level. The same airfoil section is used throughout the span, and the wing is slightly twisted. Data for this case were presented in references 25 and 26; this configuration is denoted wing A mid-mounted in those references.

Basic Computational Results

The flow about the first configuration was computed by using FLO-30 alone (i.e., inviscid calculation) and using FLO-30 interacted with the integral boundary-layer scheme, with and without the viscous wake model. The cases were run at the experimental angle of attack of 1.65° and Mach number of 0.78; the Reynolds number was 2.4×10^6 based on the mean chord.

Computed chordwise pressure distributions for the first test case configuration, taken at 24, 64, and 82 percent semispan, are compared with experiment in figure 8. The experimental stations are 26, 63, and 82 percent semispan. Agreement again is good, with cove-region and trailing-edge pressure predictions quite reasonable. Discrepancies at the upper surface leading edges of the outboard stations are noted; no explanation can be given at this time.

Isoinclines of δ^* for the first test case are shown in figure 9 for the upper and lower surfaces, respectively. Note that on the upper surface, lines of constant δ^* are for the most part parallel to the leading edge, indicating little cross flow in the boundary layer. Near midspan, however, δ^* grows more rapidly as the trailing edge is approached than in the inboard region. This strongly reduces the trailing-edge angle of the displacement body, effectively decambering this region more than inboard. Isoinclines of δ^* on the lower surface are seen to sweep forward from parallel to the leading edge after mid-

chord, indicating more rapid relative thickening of the boundary layer toward the tip. In fact, the maximum δ^*/c in the lower surface cove region is more than 30 percent greater in the outboard region than inboard. This reflects the cross flow in the boundary layer causing mass to build up toward the tip; the outboard sections are thus decambered more by viscous effects.

In figure 10 is shown a comparison between the spanwise section lift distributions from a purely inviscid calculation and the interacted calculation using the curved wake model outlined in the previous section. FLO-30 was the inviscid method used in both calculations. Also shown in the figure are experimental values of c_l obtained from integrated pressure distributions. Apparent from the figure is the large decrease in lift due to the decambering effect of the boundary layer. This decambering is stronger toward the tip than near the root. A large amount of spanwise flow occurred in the boundary layer in the lower surface cove region; therefore, this effect was expected. The interaction method with the full-wake model agrees well with experiment, with a small discrepancy near the body. This difference is probably due to incorrect modeling of the flow in the wing-body juncture region. The total lift coefficient computed for the wing-body configuration is also very close to that from experimental balance data - 0.472 computed versus 0.471 measured.

Flow about the second test case configuration was also computed by using the interaction procedure with FLO-30, the integral boundary-layer scheme, and the full wake model. Again, experimental free-stream conditions were used; the Mach number was 0.819, the angle of attack was 1.96°, and the Reynolds number was 6×10^6 based on the mean chord. Transition was fixed at 5 percent chord.

In figure 11 is shown a comparison between chordwise pressure distributions from the experimental data of references 25 and 26 and that computed with the interaction procedure. Shock strength and position are predicted well over most of the span, with a disagreement in position of a few percent chord developing toward the tip. Cove region pressures on the lower surface are also predicted reasonably well. Predicted trailing-edge pressures are slightly too high. However, the airfoil sections used in this wing have sharp trailing edges; therefore, this discrepancy cannot be attributed to inadequate modeling of blunt trailing-edge flow. These results are perhaps a good case for the development of an adequate three-dimensional strong interaction theory for wing trailing edges.

Viscous effects for the wing A test case are also fairly large, as can be seen in the comparison of interacted and inviscid chordwise pressure distributions at 68 percent semispan shown in figure 12. Without viscous correction, FLO-30 predicts the shock 0.14c too far aft and predicts a much greater cove region pressure.

Wake Effects

The results of calculations including wake effects were compared with those using the wake model of reference 19. The wake model in that procedure is modified from that incorporated in the original FLO codes only in the carrying of

the trailing-edge thickness downstream to the edge of the computational domain along the assumed wake center line. Flow tangency is not strictly satisfied at the wake, and the pressures on either side of the wake are set equal only to the order of small-disturbance theory.

In figure 13, the parameter R is plotted against span distance, where

$$R \equiv \frac{c_{l,\text{inviscid}} - c_l}{c_{l,\text{inviscid}}}$$

Thus, R is the normalized lift reduction due to viscous effects. The two curves shown in figure 13(a) are computed by using the present full wake model and by using the model of reference 19. Also shown are experimental values of R, computed using the experimental c_l's and the computed inviscid c_l's. Wake effects are thus seen to be very important in the calculation of the lift distribution on three-dimensional wings. In figure 13(b) the spanwise distributions of the lift reduction parameter R computed using the present wake model are compared with those computed using the displacement thickness of the wake only, that is, neglecting the wake curvature effects. The experimental points are again shown. Note that the wake curvature effects are strongest again near the tip and that agreement in this area is much improved by including these effects. The curvature effect of the wake is seen to be larger than the displacement effect, which is similar to the results shown in two dimensions in reference 1.

In figure 14 are compared the chordwise pressure distributions near midspan from calculations using the full and original wake models. Note that the cove region pressure predicted using the full wake model is lower than that of the original model, in better agreement with experiment.

Body Effects

An early, unpublished version of the present interaction procedure used the full-potential code FLO-27 in wing-alone mode and the original wake model coupled with the integral boundary-layer method. Gross discrepancies between predicted and experimental pressure and lift distributions were seen by using this method. A comparison between lift distributions predicted using FLO-30 with the original wake model and this early method for the first test case configuration is given in figure 15. The early method was run with a Mach number shift of 0.005 in an attempt to account for the body thickness effect. The test wing, low-mounted on a wide body, lies in a strong downwash field, which affects the predicted lift distribution significantly; less than a degree of downwash would be required to produce the lift discrepancy seen in figure 15.

Computational Efficiency

In all interaction procedures developed in this study, it was found that the additional computational work required to converge a viscous-inviscid interaction case over that needed to converge the same case using the inviscid procedure alone was comparatively small. Also, inclusion of the wake effects was found to give no convergence penalty in the interaction procedure. With the full wake model, in fact, by properly selecting the δ^* underrelaxation factor and the scheduling of the number of inviscid fine-grid iterations between viscous updates, the total number of fine-grid iterations required to converge an interacted case was only slightly greater than that required to converge a purely inviscid case to the same residual level. To converge to a level where the maximum residual in the field was 1.5×10^{-5}, the purely inviscid run required the work equivalent of 728 fine-grid iterations on a halving sequence of three grids. The interacted test case required the equivalent of 756 fine-grid iterations. For the first two inviscid computations in the interaction sequence, calculation was begun afresh on the coarsest grid. Starting with the third iteration, the solution was restarted on the finest grid and a relatively small number of fine-grid iterations were run per viscous update. A total of seven global iterations were required, and a δ^* underrelaxation factor of 0.6 was used. Another interesting statistic is that, of the total CP time spent converging an interacted case, only 3 percent is spent computing the viscous parameters by using the integral method, compared with over 50 percent for the method of reference 6.

CONCLUDING REMARKS

A viscous-inviscid interaction computational method has been developed for three-dimensional transonic wing-body configurations. The procedure employs a three-dimensional integral boundary-layer method for viscous correction on the wing surfaces which produces results in good agreement with a finite-difference method in a fraction of the computer time. The integral method is stable and robust and incorporates a model for computation in a small region of streamwise separation. A locally two-dimensional wake model, accounting for thickness and curvature effects, is also included in the interaction procedure. Computation time spent in converging an interacted result is, many times, only a small amount greater than that required to converge an inviscid calculation to the same maximum residual.

Results for test cases in which viscous effects are large have shown good agreement with experimental data. In particular, the use of the full-wake model improved the prediction of spanwise load distribution and cove region pressure over results by using the wake model originally employed in FLO-30. For transonic wing-body configurations, it is also apparent that body effects may be large. It is seen that a three-dimensional boundary-layer method must be used

on the wing, rather than a two-dimensional strip method, in order to properly predict the increased decambering of the sections near the tip, due to cross flow in the boundary layer.

Langley Research Center
National Aeronautics and Space Administration
Hampton, VA 23665
July 29, 1981

REFERENCES

1. Melnik, R. E.; Chow, R.; and Mead, H. R.: Theory of Viscous Transonic Flow Over Airfoils at High Reynolds Number. AIAA Paper No. 77-680, June 1977.

2. Melnik, R. E.; and Grossman, B.: On the Turbulent Viscid-Inviscid Interaction at a Wedge Shaped Trailing Edge. Grumman paper presented at Symposium on Numerical and Physical Aspects of Aerodynamic Flows (California State University, Long Beach), Jan. 19-21, 1981.

3. Newman, Perry A.; Carter, James E.; and Davis, Ruby M.: Interaction of a Two-Dimensional Strip Boundary Layer With a Three-Dimensional Transonic Swept-Wing Code. NASA TM-78640, 1978.

4. Waggoner, E. G.: Computational Transonic Analysis for a Supercritical Transport Wing-Body Configuration. AIAA-80-0129, Jan. 1980.

5. Kjelgaard, Scott O.; and Thomas, James L.: Comparison of Three-Dimensional Panel Methods With Strip Boundary-Layer Simulations to Experiment. NASA TM-80088, 1979.

6. McLean, J. D.; and Randall, J. L.: Computer Program To Calculate Three-Dimensional Boundary Layer Flows Over Wings With Wall Mass Transfer. NASA CR-3123, 1979.

7. Coles, Donald: The Law of the Wake in Turbulent Boundary Layers. J. Fluid Mech., vol. 1, pt. 2, July 1956, pp. 191-226.

8. Stock, H. W.: Integral Method for the Calculation of Three-Dimensional, Laminar and Turbulent Boundary Layers. NASA TM-75320, 1978.

9. Smith, P. D.: An Integral Prediction Method for Three-Dimensional Compressible Turbulent Boundary Layers. R. & M. No. 3739, British A.R.C., 1974.

10. Tetervin, Neal; and Lin, Chia Chiao: A General Integral Form of the Boundary-Layer Equation for Incompressible Flow With an Application to the Calculation of the Separation Point of Turbulent Boundary Layers. NACA Rep. 1046, 1951. (Supersedes NACA TN 2158.)

11. Mager, Artur: Generalization of Boundary-Layer Momentum-Integral Equations to Three-Dimensional Flows Including Those of Rotating System. NACA Rep. 1067, 1952. (Supersedes NACA TN 2310.)

12. Schlichting, Hermann (J. Kestin, transl.): Boundary-Layer Theory, Sixth ed. McGraw-Hill Book Co., Inc., c.1968.

13. Green, J. E.; Weeks, D. J.; and Brooman, J. W. F.: Prediction of Turbulent Boundary Layers and Wakes in Compressible Flow by a Lag-Entrainment Method. R. & M. No. 3791, British A.R.C., 1977.

14. Myring, D. F.: An Integral Prediction Method for Threedimensional Turbulent Boundary Layers in Incompressible Flow. Tech. Rep. 70147, British R.A.E., Aug. 1970.

15. Roache, Patrick J.: Computational Fluid Dynamics. Hermosa Publishers, c.1972.

16. Cumpsty, N. A.; and Head, M. R.: The Calculation of Three-Dimensional Turbulent Boundary Layers. Part II: Attachment-Line Flow on an Infinite Swept Wing. Aeronaut. Q., vol. XVIII, pt. II, May 1967, pp. 150-164.

17. Stanewsky, E.; Puffert, W.; Muller, R.; and Bateman, T. E. B.: Supercritical Airfoil CAST 7 - Surface Pressure, Wake and Boundary Layer Measurements. Experimental Data Base for Computer Program Assessment, AGARD-AR-138, May 1979, pp. A3-1 - A3-35.

18. Jameson, Antony: Iterative Solution of Transonic Flows Over Airfoils and Wings, Including Flows at Mach 1. Commun. Pure & Appl. Math., vol. XXVII, no. 3, May 1974, pp. 283-309.

19. Caughey, D. A.; and Jameson, A.: Recent Progress in Finite-Volume Calculations for Wing-Fuselage Combinations. AIAA Paper 79-1513, July 1979.

20. Caughey, David A.; Newman, Perry A.; and Jameson, Antony: Recent Experiences With Three-Dimensional Transonic Potential Flow Calculations. NASA TM-78733, 1978.

21. Jameson, Antony; and Caughey, D. A.: A Finite Volume Method for Transonic Potential Flow Calculations. A Collection of Technical Papers - AIAA 3rd Computational Fluid Dynamics Conference, June 1977, pp. 35-54. (Available as AIAA Paper 77-635.)

22. Lock; R. C.: Calculations of Viscous Effects on Aerofoils in Compressible Flow. Tech. Memo. Aero 1646, British R.A.E., Sept. 1975.

23. Moore, Franklin K.: Displacement Effect of a Three-Dimensional Boundary Layer. NACA Rep. 1124, 1953. (Supersedes NACA TN 2722.)

24. Bartlett, Dennis W.: Wind-Tunnel Investigation of Several High Aspect-Ratio Supercritical Wing Configurations on a Wide-Body Type Fuselage. NASA TM X-71996, 1977.

25. Hinson, B. L.; and Burdges, K. P.: Acquisition and Application of Transonic Wing and Far-Field Test Data for Three-Dimensional Computational Method Evaluation. AFOSR-TR-80-0421, U.S. Air Force, Mar. 1980. (Available from DTIC as AD A085 258.)

26. Hinson, B. L.; and Burdges, K. P.: Acquisition and Application of Transonic Wing and Far-Field Test Data for Three-Dimensional Computational Method Evaluation. Volume II - Appendix B, Experimental Data. AFOSR-TR-80-0422, U.S. Air Force, Mar. 1980. (Available from DTIC as AD A085 259.)

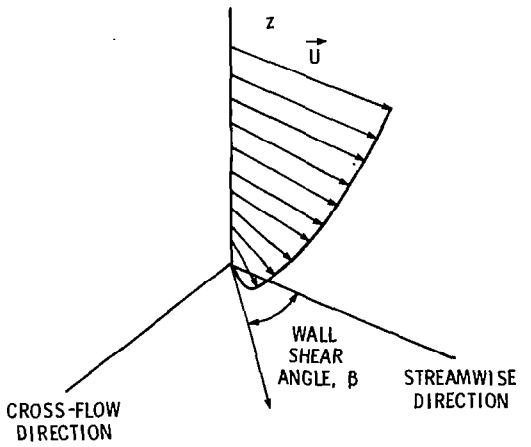

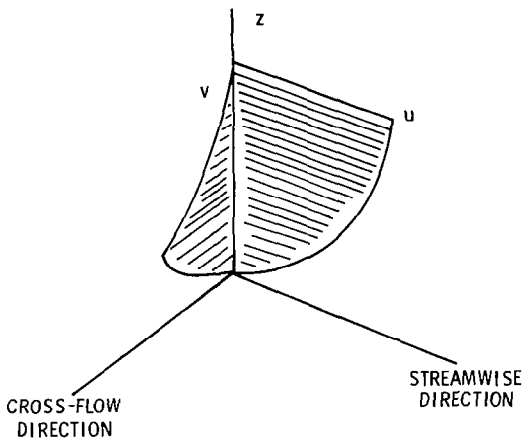

Figure 1.- Breakdown of three-dimensional boundary layer into components.

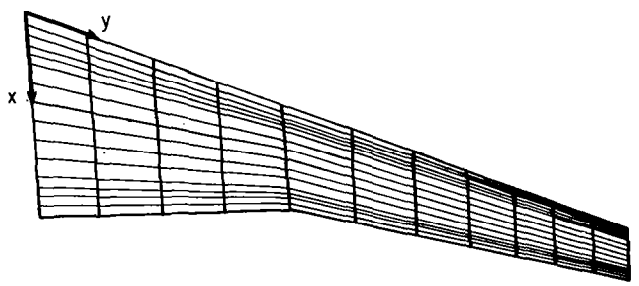

Figure 2.- Boundary-layer grid.

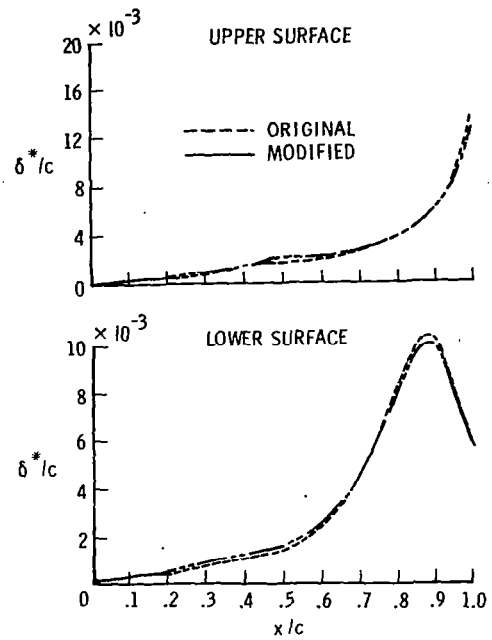

Figure 3.- Comparison of displacement thickness predictions for $\eta = 0.6$.

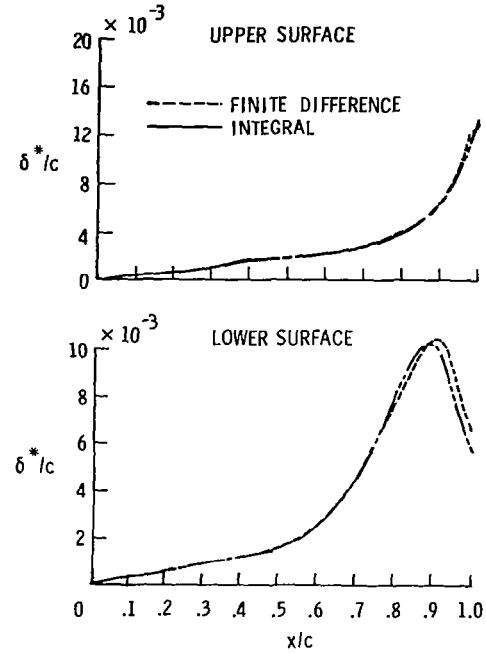

Figure 4.- Comparison of displacement thickness predictions for $\eta = 0.7$.

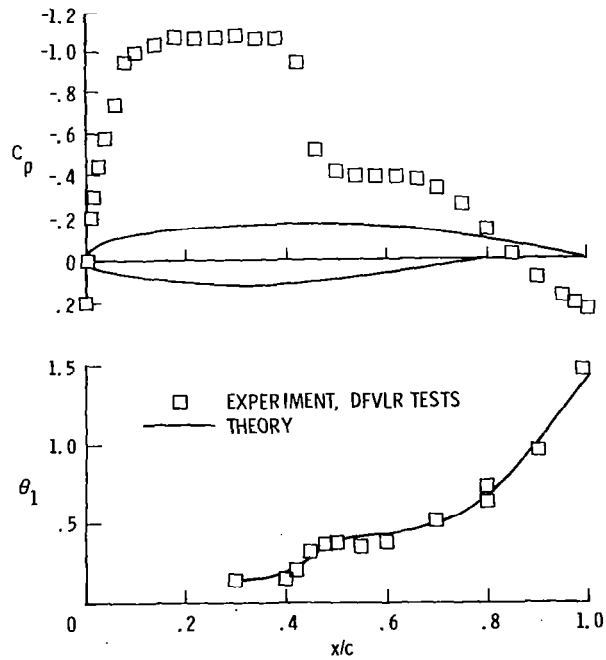

Figure 5.- Comparison with experiment for two-dimensional boundary layer only. $M = 0.76$; $N_{Re,c} = 2.4 \times 10^6$.

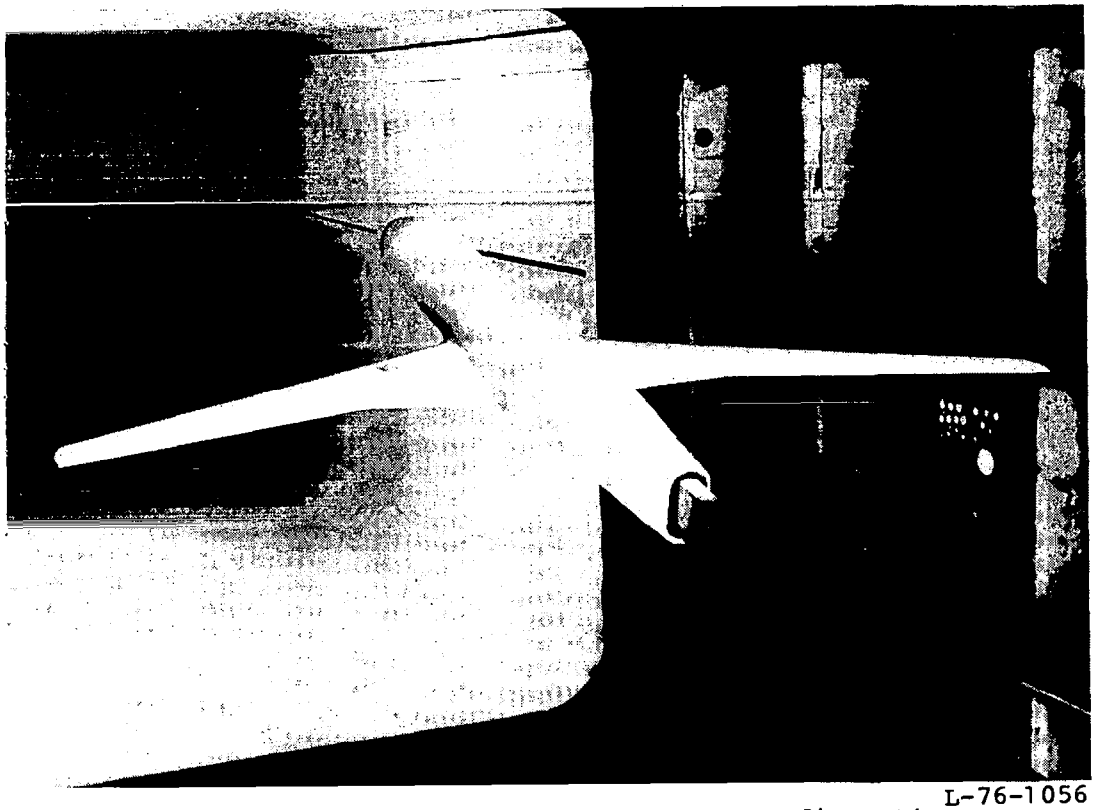

L-76-1056

Figure 6.- Advanced transport test case configuration.

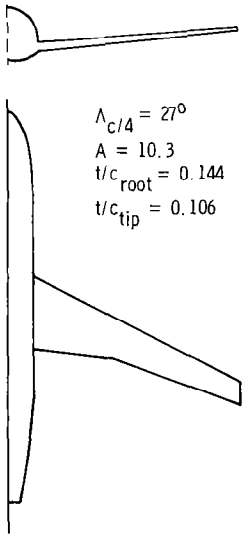

(a) Advanced transport.

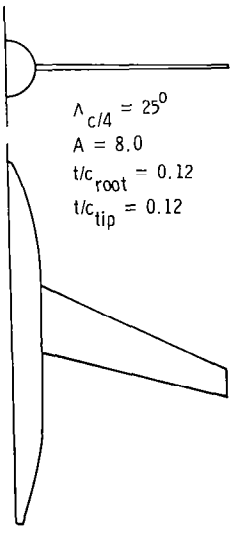

(b) Wing A from references 25 and 26.

Figure 7.- Test case configurations.

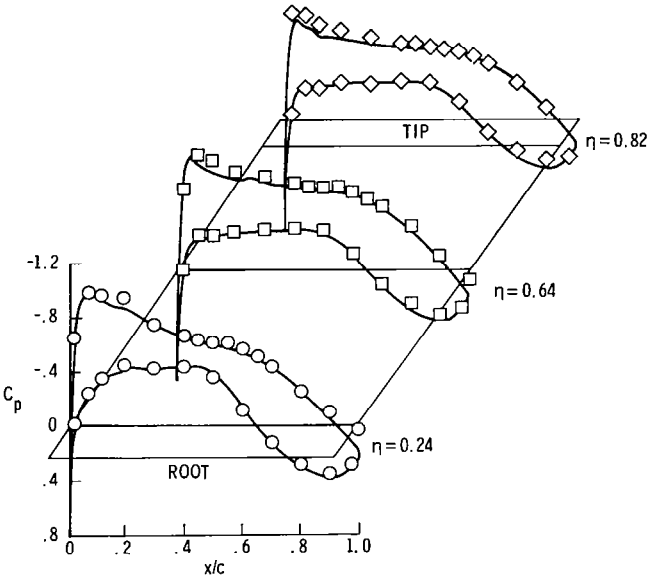

Figure 8.- Chordwise pressure distributions for advanced transport configuration. Experimental data (symbols) from reference 24.

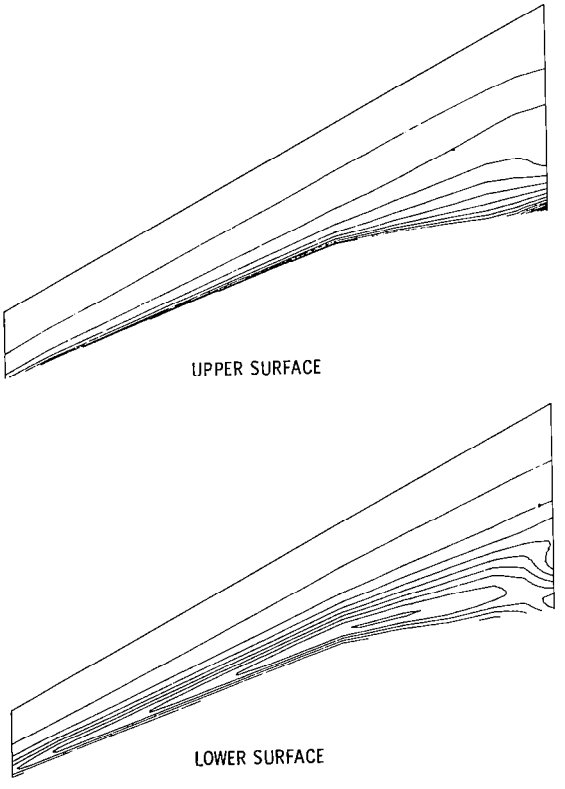

Figure 9.- Isoinclines of δ^* for advanced transport configuration.

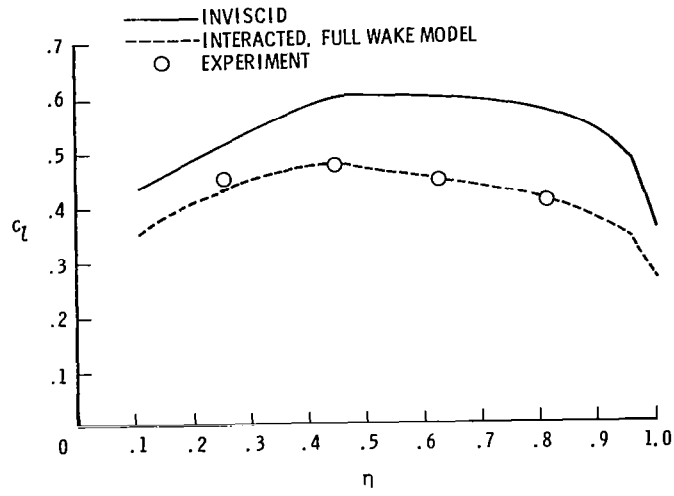

Figure 10.- Spanwise lift distribution for advanced transport configuration.

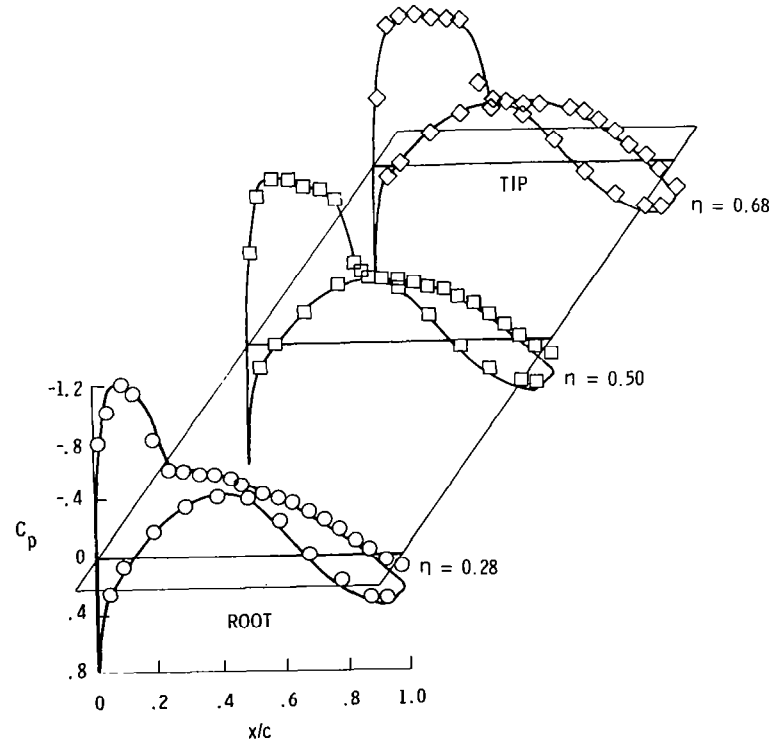

Figure 11.- Chordwise pressure distributions for wing A test configuration. Experimental data (symbols) from references 25 and 26.

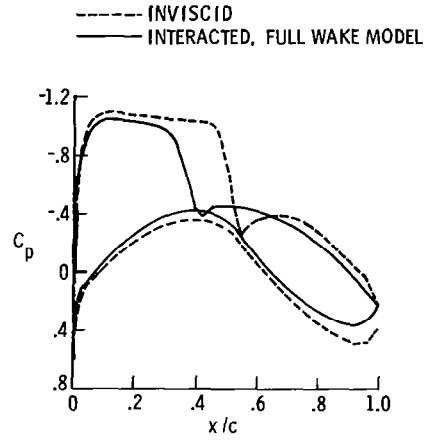

Figure 12.- Comparison of chordwise pressure distributions for wing A test configuration. $\eta = 0.68$.

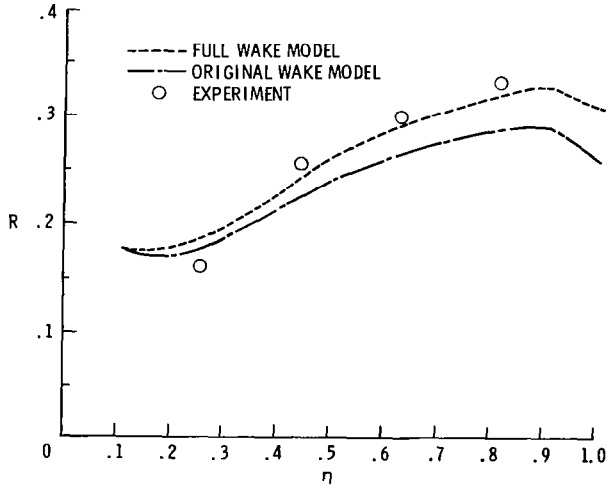

(a) Wake displacement and curvature effect.

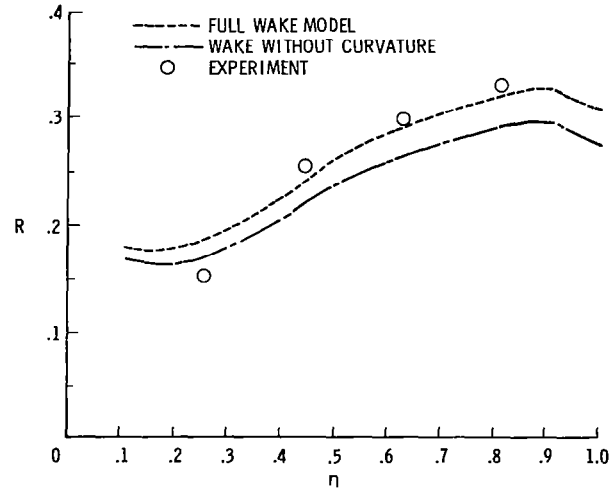

(b) Wake curvature effect.

Figure 13.- Lift reduction parameter plotted against span for advanced transport configuration.

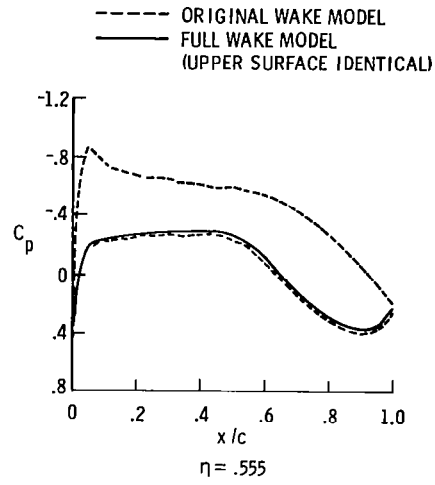

Figure 14.- Chordwise pressure distributions for advanced transport configuration. η = 0.56.

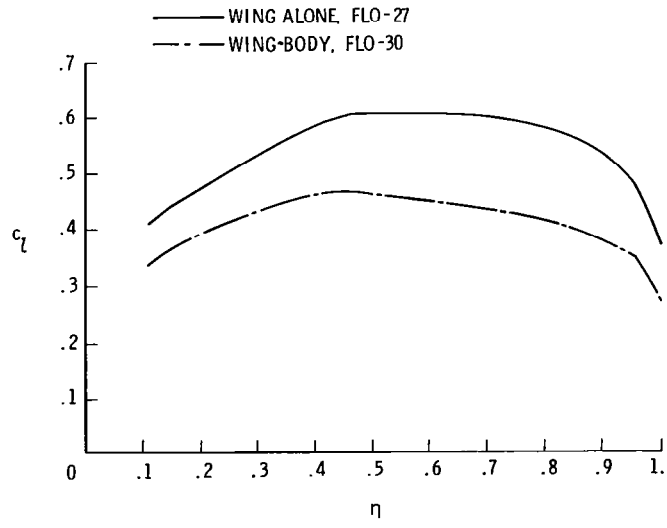

Figure 15.- Influence of fuselage on spanwise lift distributions for advanced transport configuration. Boundary layer interaction only.

1. Report No.	2. Government Accession No.	3. Recipient's Catalog No.
NASA TP-1910		

4. Title and Subtitle	5. Report Date
VISCOUS-INVISCID INTERACTION METHOD INCLUDING WAKE EFFECTS FOR THREE-DIMENSIONAL WING-BODY CONFIGURATIONS	SEPTEMBER 1981
	6. Performing Organization Code 505-31-13-01
7. Author(s) Craig L. Streett	8. Performing Organization Report No. L-14053
	10. Work Unit No.
9. Performing Organization Name and Address NASA Langley Research Center Hampton, VA 23665	11. Contract or Grant No.
	13. Type of Report and Period Covered Technical Paper
12. Sponsoring Agency Name and Address National Aeronautics and Space Administration Washington, DC 20546	14. Sponsoring Agency Code

15. Supplementary Notes

A condensed version of this report was presented at the AIAA 14th Fluid and Plasma Dynamics Conference at Palo Alto, California, June 22-24, 1981, and is available as AIAA Paper No. 81-1266.

16. Abstract

A viscous-inviscid interaction method has been developed by using a three-dimensional integral boundary-layer method which produces results in good agreement with a finite-difference method in a fraction of the computer time. The integral method is stable and robust and incorporates a model for computation in a small region of streamwise separation. A locally two-dimensional wake model, accounting for thickness and curvature effects, is also included in the interaction procedure. Computation time spent in converging an interacted result is, many times, only slightly greater than that required to converge an inviscid calculation. Results are shown from the interaction method, run at experimental angle of attack, Reynolds number, and Mach number, on a wing-body test case for which viscous effects are large. Agreement with experiment is good; in particular, the present wake model improves prediction of the spanwise lift distribution and lower surface cove pressure.

17. Key Words (Suggested by Author(s))	18. Distribution Statement
Three-dimensional boundary layer Viscous-inviscid interaction Wing-body configurations Transonic flow Supercritical wings Computational fluid dynamics	FEDD Distribution Subject Category 02

19. Security Classif. (of this report)	20. Security Classif. (of this page)	21. No. of Pages	22.
Unclassified	Unclassified	28	

Available: NASA's Industrial Applications Centers

NASA-Langley, 1981